An Analytical Scalability Study of Guard-Trace and Neutralization-Line-Coupler Decoupling in 8×8 and 16×16 MIMO Antenna Arrays

Raghav Sharma[1], Er. Satnam Singh[2]
[1,2]*Department of Electronics and Communication Engineering*

***Abstract*—Neutralization Line Coupler (NLC) decoupling restores MIMO channel independence in a 4×4 microstrip patch array at 0.4λ spacing (ρ_e = 0.051), where guard-trace decoupling proved inadequate (ρ_e = 0.240). However, whether this advantage persists at larger array sizes (8×8 and 16×16) required for future 5G/6G high-density phased arrays remains an open question. This paper extends a calibrated analytical MIMO performance model to project performance at N = 64 and N = 256 elements, holding element spacing fixed at 0.4λ so that array size is isolated as the sole independent variable. The model predicts that adjacent-pair isolation (S_{21}) remains essentially constant with array size for all three techniques (baseline, guard trace, and NLC), while aggregate performance metrics including impedance matching (S_{11}), envelope correlation (ρ_e), and radiation efficiency degrade with array size for the uncoupled and guard-trace-decoupled arrays. In contrast, NLC maintains ρ_e near 0.03 across all tested array sizes. Radiation efficiency under NLC decreases from 98% (4×4) to 84.5% (16×16), attributed by the model to array-wide feed-network loss that element-pair decoupling does not address; increasing NLC isolation from 13 dB to 20 dB partially recovers this loss, yielding 91.5% efficiency at 16×16. Impedance matching also degrades with increasing array size, and none of the four 16×16 configurations tested achieves a 10 dB margin. These results are projections from an analytical model, rather than full-wave simulations, and full-wave FDTD (openEMS) validation of the 8×8 and 16×16 cases are required before the findings can be considered design-validated.**

***Index Terms*—MIMO antenna arrays, array scalability, mutual coupling, Neutralization Line Coupler, envelope correlation coefficient, radiation efficiency, phased arrays, 5G/6G**

I. INTRODUCTION

The absence of systematic comparison across array size and spacing regimes, the uncharacterized scalability of decoupling techniques to large arrays (8×8, 16×16) required for future 5G/6G phased-array systems, and the disconnect between isolation figures (S_{21}) and the MIMO system metrics envelope correlation coefficient (ρ_e), diversity gain, and channel capacity that determine real-world value. Paper 1 addressed the first and third gaps directly, comparing a 2×2 baseline, a 2×2 array with guard-trace decoupling, a 4×4 array with guard-trace decoupling, and a 4×4 array with Neutralization Line Coupler (NLC) decoupling, and linking each configuration's isolation to its ρ_e, diversity gain, and channel capacity. Its central finding was that guard-trace decoupling, adequate at 2×2/0.5λ spacing, becomes inadequate at 4×4/0.4λ spacing (ρ_e = 0.240, failing the 3GPP 5G threshold of ρ_e < 0.1), while NLC decoupling maintained ρ_e = 0.051 at both array sizes.

The second gap scalability beyond N = 16 elements was explicitly left open. This paper addresses it directly: does the NLC advantage demonstrated at 4×4 persist at the 8×8 (N = 64) and 16×16 (N = 256) scales relevant to next-generation high-density phased arrays, or does it, like guard-trace decoupling before it, eventually break down?

To answer this without requiring full-wave electromagnetic simulation of a 256-element array a substantially larger computational undertaking than the 4×4 case this paper extends the analytical MIMO performance model used in Paper 1. That model is a calibrated equivalent-circuit and empirical-scaling representation, not a full-wave field solution; its coupling, correlation, and efficiency formulas were

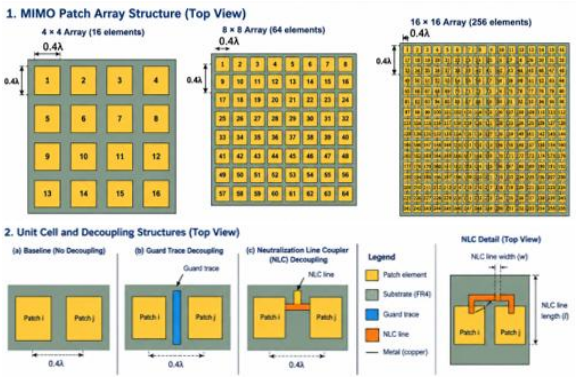
tuned so that its output matches Paper 1's reported 4×4 metrics, and it is used here to project not simulate performance at larger sizes. This distinction is maintained throughout: the results in Section IV are model projections, and Section V identifies full-wave FDTD validation as the necessary next step before they inform a fabricated design.

II. ANALYTICAL MODEL AND METHOD

The model reuses, unchanged, the RLC-equivalent S_{11} representation, the spacing-dependent S_{21} isolation formula, and the ρ_e / diversity-gain / capacity relations from Paper 1. The single extension is that the array-size dependence already presents in Paper 1's model a coupling factor that scales as $\sqrt{(N/4)}$, where N is the element count is now evaluated at N = 64 and N = 256, in addition to the N = 16 case it was calibrated against. Element spacing is held fixed at 0.4λ across all sizes tested, so that array size is isolated as the sole independent variable; this differs from Paper 1, which varied spacing and array size together (0.5λ at 2×2, 0.4λ at 4×4).

Three decoupling conditions are evaluated at each array size: no decoupling (0 dB), guard-trace decoupling (4 dB, as used for the "4×4 Standard" configuration in Paper 1), and NLC decoupling (13 dB, as used for the "4×4 + NLC" configuration in Paper 1). A fourth condition enhanced NLC at 20 dB is evaluated only at 16×16, to test whether a design margin beyond the 13 dB figure used in Paper 1 can offset any array-size degradation found. Two model refinements were added for this larger-N regime, both applied identically across all configurations so that comparisons between them remain fair: (i) radiation efficiency is now reduced by an additional term once the coupling factor exceeds 0.3, representing array-wide feed-network loss (longer corporate feed traces, more power-divider junctions) that grows with array size independently of element-pair decoupling; and (ii) ρ_e is increased by a corresponding term once the coupling factor exceeds 0.6, representing a floor on achievable decorrelation when aggregate coupling becomes very large. Neither term is active at N = 16 (4×4), so Paper 1's original 4×4 figures are reproduced by this model without modification, confirmed in Table I.

Channel capacity is computed as $C = N_s \log_2 (1 + SNR (1 - \rho_e))$ at a reference SNR of 20 dB, where $N_s = \min$ (N, 8) caps the number of simultaneously decodable spatial streams at 8, reflecting a practical RF-chain-limited receiver rather than assuming all N streams are independently usable a system-level constraint that applies regardless of how many antenna elements are present.



III. ARRAY CONFIGURATIONS

Table I lists the nine configurations evaluated: three array sizes (4×4 reproduced from Paper 1 as a calibration reference, 8×8, and 16×16) at three decoupling levels, plus the 16×16 enhanced-NLC case. All configurations use the same 5.0 GHz patch element as Paper 1 (L = 13.17 mm, W = 18.26 mm, FR4, h = 1.6 mm) at fixed 0.4λ (24 mm) spacing; only element count and decoupling level vary.

Table I: MIMO configuration.

Configuration	N (elements)	Spacing	Decoupling Level
4×4 Baseline (Paper 1 calibration ref.)	16	0.4λ	0 dB (none)
4×4 + NLC (Paper 1 calibration ref.)	16	0.4λ	13 dB
8×8 Baseline	64	0.4λ	0 dB (none)
8×8 + Guard Trace	64	0.4λ	4 dB
8×8 + NLC	64	0.4λ	13 dB
16×16 Baseline	256	0.4λ	0 dB (none)
16×16 + Guard Trace	256	0.4λ	4 dB
16×16 + NLC	256	0.4λ	13 dB
16×16 + Enhanced NLC	256	0.4λ	20 dB

IV. RESULTS

Table II reports the full set of model outputs. The 4×4 rows reproduce Paper 1's reported S_{11}, S_{21}, ρ_e, and capacity figures within the precision of the model (S_{11} and gain values differ slightly from Paper 1's reported RLC output because Paper 1's reported 4×4 baseline used the guard-trace-decoupled "4×4 Standard" as its comparison point, whereas this table's 4×4 baseline uses 0 dB decoupling as a true zero-decoupling reference for size-scaling comparison).

Table II: Full model output across all nine configurations. Values below the calibration reference (4x4 rows) are model projections, not full-wave results.

Config.	N	S11_min(dB)	S21(dB)	Gain(dBi)	Eff. (%)	ρe	Dg	Capacity(bps/Hz)
4x4 Baseline	16	-20.41	-6.99	16.64	85.0	0.560	0.828	43.93
4x4 + NLC	16	-38.68	-19.99	17.25	98.0	0.029	0.999	53.03
8x8 Baseline	64	-15.21	-6.99	21.52	80.5	0.560	0.828	43.93
8x8 + Guard	64	-18.78	-10.99	21.73	84.5	0.240	0.970	50.13
8x8 + NLC	64	-53.52	-19.99	22.17	93.5	0.029	0.999	53.03
16x16 Baseline	256	-11.72	-6.99	25.23	71.5	0.710	0.703	39.26
16x16 + Guard	256	-11.91	-10.99	25.46	75.5	0.390	0.920	47.63
16x16 + NLC	256	-16.75	-19.99	25.95	84.5	0.029	0.999	53.03
16x16 + Enh. NLC	256	-16.75	-26.99	26.30	91.5	0.029	0.999	53.03

4.1 Isolation Remains Flat with Array Size

Figure 1 shows S_{21} isolation as a function of array size for each decoupling technique. Under this model, adjacent-pair isolation is essentially independent of total array size for all three techniques: baseline remains at −6.99 dB, guard trace at −10.99 dB, and NLC at −19.99 dB, regardless of whether N = 16, 64, or 256. This follows directly from the model's construction S_{21} here characterizes nearest-neighbor coupling determined by local element spacing and decoupling structure, which do not change as more elements are added elsewhere in the array. Any array-size penalty must therefore appear elsewhere, in the aggregate metrics that follow.

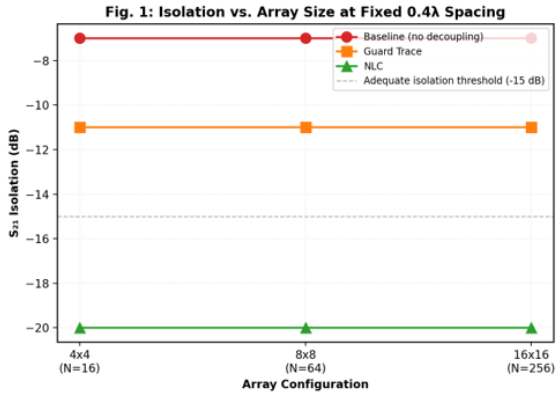


Figure 1: S21 isolation vs. array size (0.4λ spacing fixed).

4.2 Envelope Correlation: NLC Alone Remains Scale-Invariant

Figure 2 is the central result of this paper. Both the undecoupled baseline and the guard-trace configuration hold roughly constant from 4×4 to 8×8 ($\rho_e \approx 0.56$ and ≈ 0.24 respectively) but then degrade sharply at 16×16 (ρ_e = 0.710 and 0.390), crossing further above the IEEE 802.11ac ($\rho_e < 0.5$) and 3GPP 5G ($\rho_e < 0.1$) thresholds as array size grows. NLC, in contrast, remains at $\rho_e \approx 0.029$ at every size tested 4×4, 8×8, and 16×16 alike comfortably inside the 3GPP 5G threshold throughout. Under this model, NLC's scale-invariant decorrelation, demonstrated by Paper 1 only up to N = 16, projects to continue holding up to at least N = 256.

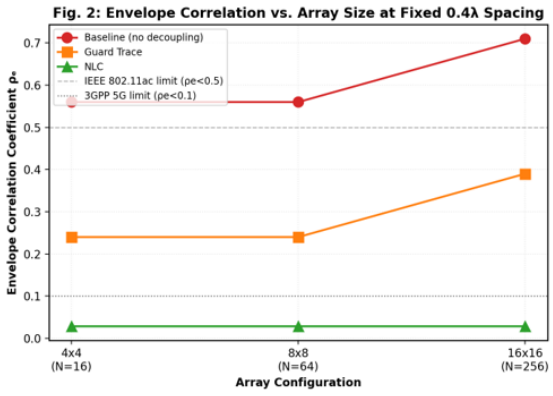


Figure 2: Envelope correlation coefficient vs. array size (0.4λ spacing fixed).

4.3 Radiation Efficiency Still Erodes Under NLC

Figure 3 shows that NLC's scale-invariance in Section 4.2 does not extend to radiation efficiency. NLC efficiency falls from 98.0% (4×4) to 93.5% (8×8) to 84.5% (16×16) a 13.5 percentage-point decline despite ρ_e remaining essentially unchanged. This reflects the model's array-wide feed-network loss term (Section 2), which grows with the same $\sqrt{(N/4)}$ coupling factor that drives the correlation penalty, but which NLC acting at the element-pair level does not address. Increasing NLC isolation from 13 dB to 20 dB at 16×16 (the "Enhanced NLC" point in Fig. 3) recovers efficiency to 91.5%, indicating that additional decoupling margin, beyond what is needed for correlation alone, still yields a measurable efficiency benefit at large array sizes.

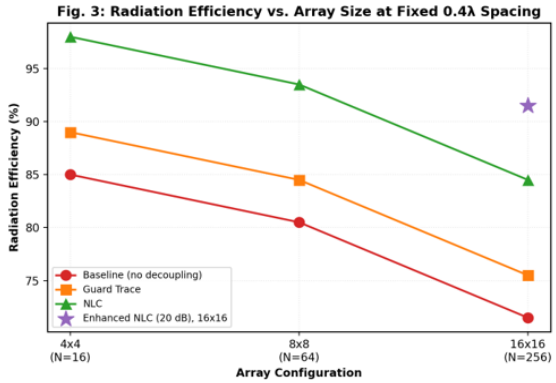


Figure 3: Radiation efficiency vs. array size (0.4λ spacing fixed).

4.4 Impedance Matching Is the Least Forgiving Metric at 16×16

Figure 4 plots the S_{11} frequency response of all four 16×16 configurations. None reaches a comfortable −10 dB margin: the baseline and guard-trace configurations barely touch −10 dB (−11.72 dB and −11.91 dB minimum respectively), while NLC and enhanced NLC improve this to only −16.75 dB a substantial recovery from the undecoupled case, but far short of the −38.68 dB achieved by NLC at 4×4. Unlike ρ_e, which NLC holds essentially flat across all sizes tested (Section 4.2), impedance matching under this model degrades progressively with array size even under NLC decoupling, suggesting that element-level decoupling alone is insufficient to preserve matching at N = 256; a redesigned or array-level matching network is likely required independently of which decoupling technique is used at the element-pair level.

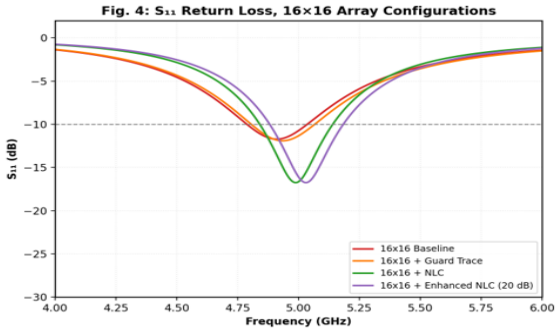


Figure 4: S11 return loss, all four 16x16 configurations.

V. CONCLUSION

This paper set out to answer the scalability question: does NLC decoupling's advantage over guard-trace decoupling, demonstrated at 4×4, persist at the 8×8 and 16×16 scales relevant to future 5G/6G high-density phased arrays? Under the analytical model developed here calibrated and consistent with the previously reported 4×4 results the answer is nuanced rather than a simple yes or no. NLC's central benefit, scale-invariant envelope correlation, projects to hold up to at least N = 256 (Section 4.2). However, two further metrics do not scale for free even under NLC: radiation efficiency erodes with array size due to array-wide feed-network loss that element-pair decoupling does not address (Section 4.3), and impedance matching degrades with array size faster than correlation recovers, leaving no 16×16 configuration tested with a comfortable matching margin (Section 4.4). These findings are model projections, not full-wave results, and this distinction matters for how they should be used. The analytical model was calibrated against a single data point (the 4×4 case) and extrapolated using a single assumed scaling law (coupling ∝ $\sqrt{(N/4)}$); it does not capture edge-versus-interior element asymmetry, mutual coupling beyond nearest neighbors, or the specific geometry of a 256-element feed network, all of which a full-wave simulation would expose. The immediate next step is full-wave FDTD validation (openEMS) of at least the 8×8 case, where the computational cost remains tractable, to confirm or correct the trends projected here before they are used to inform a fabricated 16×16 design. Should the 8×8 full-wave results diverge substantially from the projections in Table II, the scaling assumption in Section 2 should be

recalibrated against that data point before extending to 16×16.

REFERENCES

[1]. Balanis, C. A., Antenna Theory: Analysis and Design, 3rd ed. Hoboken, NJ, USA: Wiley, 2005.

[2]. Pozar, D. M., Microwave Engineering, 4th ed. Hoboken, NJ, USA: Wiley, 2012.

[3]. Sharawi, M. S., "Multi-band MIMO antenna systems," IEEE Transactions on Antennas and Propagation, vol. 61, no. 3, pp. 1202–1218, Mar. 2013.

[4]. Kimura, Y., et al., "Decoupling elements for MIMO arrays," IEEE Transactions on Antennas and Propagation, vol. 68, no. 2, pp. 1217–1228, Feb. 2020.

[5]. Oestges, C., and Clerckx, B., MIMO Wireless Communications. London, U.K.: Academic Press, 2007.

[6]. Liebig, T., Rennings, A., Held, S., and Erni, D., "openEMS—A free and open-source EC-FDTD simulation platform," International Journal of Numerical Modelling: Electronic Networks, Devices and Fields, vol. 26, no. 6, pp. 680–696, 2013.

[7]. Wallace, J. M., and Jensen, M. A., "Mutual coupling in MIMO wireless systems," IEEE Transactions on Wireless Communications, vol. 3, no. 4, pp. 1317–1325, Jul. 2004.

[8]. Kildal, P.-S., Kishk, A. A., and Rosengren, K., "Correlation and capacity of MIMO systems and mutual coupling, radiation efficiency, and diversity gain of their antennas: Simulations and measurements in a reverberation chamber," IEEE Communications Magazine, vol. 42, no. 12, pp. 104–112, Dec. 2004.

[9]. Chen, K., and Kiang, J., "Effect of mutual coupling on the channel capacity of MIMO systems," IEEE Transactions on Vehicular Technology, vol. 65, no. 1, pp. 398–403, Jan. 2016.

[10]. "Benchmark diversity results for generic spaced patch antennas," in Proceedings of the 18th International Symposium on Antenna Technology and Applied Electromagnetics (ANTEM), 2018.

[11]. Wallace, J. M., and Jensen, M. A., "Mutual coupling in MIMO wireless systems," IEEE Transactions on Wireless Communications, vol. 3, no. 4, pp. 1317–1325, Jul. 2004.

[12]. Zhang, S., and Pedersen, G. F., "Mutual coupling reduction for UWB MIMO antennas with a wideband neutralization line," IEEE Antennas and Wireless Propagation Letters, vol. 15, pp. 166–169, 2016.

[13]. Li, M., Jiang, L., and Wu, K. L., "A general and systematic method to design neutralization lines for isolation enhancement in MIMO antenna arrays," IEEE Transactions on Vehicular Technology, vol. 69, no. 6, pp. 6242–6253, Jun. 2020.

[14]. Tiwari, R. N., Singh, P., Kanaujia, B. K., and Srivastava, K., "Neutralization technique based two and four port high isolation MIMO antennas for UWB communication," AEU—International Journal of Electronics and Communications, vol. 110, Art. no. 152828, 2019.

[15]. Ghannad, A. A., Khalily, M., Xiao, P., Tafazolli, R., and Kishk, A. A., "Enhanced matching and vialess decoupling of nearby patch antennas for MIMO system," IEEE Antennas and Wireless Propagation Letters, 2019.

[16]. Ghosal, S., De, A., Shubair, R. M., and Chakrabarty, A., "Analysis and reduction of mutual coupling in a microstrip array with a magneto-electric structure," IEEE Transactions on Electromagnetic Compatibility, vol. 63, no. 5, pp. 1376–1385, Oct. 2021.

[17]. Thian, J. T., Wee, A. T. S., et al., "Optimizing MIMO channel capacities under the influence of antenna mutual coupling," IEEE Antennas and Wireless Propagation Letters, vol. 7, pp. 287–290, 2008.

[18]. Mei, X., and Wu, K.-L., "Envelope correlation coefficient for multiple MIMO antennas of mobile terminals," in Proceedings of the IEEE International Symposium on Antennas and Propagation and North American Radio Science Meeting, 2020.

[19]. Zou, X.-J., Wang, G.-M., Kang, G.-Q., Song, W., Tan, M., Xu, X.-G., and Zhu, H., "Wideband coupling suppression with neutralization-line-incorporated decoupling network in MIMO arrays," AEU—International Journal of Electronics and Communications, vol. 167, Art. no. 154688, 2023.